Journal of Materials Chemistry A

ROYAL SOCIETY OF CHEMISTRY

PAPER

View Article Online
View Journal | View Issue

Cite this: *J. Mater. Chem. A*, 2020, **8**, 4562

Effect of conjugated polymer electrolytes with diverse acid derivatives as a cathode buffer layer on photovoltaic properties†

Ho Cheol Jin,‡[a] Sabrina Aufar Salma,‡[a] Doo Kyung Moon [b] and Joo Hyun Kim *[a]

We fabricated and tested inverted polymer solar cells (PSCs) that use a blend of PTB7-Th and $PC_{71}BM$ as the active layer and poly[(9,9-bis(3′-(*N*,*N*-dimethylamino)propyl)-2,7-fluorene)-*alt*-2,7-(9,9-dihexylfluorene)] (PFN) with different amounts and types of acid derivatives as the cathode buffer layer to systematically study the effect of amounts and types of acid additives such as acetic acid (AA), 4-trifluoromethyl benzoic acid (CF3BA), trifluoroacetic acid (CF3AA), and 4-toluene sulfonic acid (TsOH) on the device performances. Consequently, a significant improvement was obtained for the device based on ZnO/PFN with 1.0 equivalent (eq.) of acid derivatives. The PCE of the device with 1.0 equivalent of AA, CF3BA, CF3AA, and TsOH was 9.9, 10.3, 10.3, and 10.6% respectively, whereas the power conversion efficiency (PCE) of the device with pristine ZnO was 8.7%. The performances of the devices followed the trend of the acid dissociation constant of acid derivatives. In addition, we discovered that the most effective acid derivative is TsOH. Furthermore, we observed that the devices based on PFN with acid derivatives exhibited reduced trap-assisted recombination and interfacial bimolecular recombination. Furthermore, reduced trap-assisted recombination of the devices agreed well with the trend of the PCEs of PSCs and followed the trend of the acid dissociation constant of acid derivatives.

Received 26th November 2019
Accepted 1st February 2020

DOI: 10.1039/c9ta12931f

rsc.li/materials-a

Introduction

In the past few decades, polymer solar cells (PSCs) have attracted a lot of attention because they are capable of being promising energy resources in the future. PSCs can be particularly advantageous in large scale applications where roll-to-roll is used because they are flexible and light-weight. Recently, the power conversion efficiency (PCE) of PSCs reached up to 16%, and this can be achieved by synthesizing donor and acceptor materials (*i.e.*, photoactive materials),[1–11] control of the morphology of the photoactive layer,[12–16] and engineering the electrode interface. Currently, the studies on PSCs are mainly focused on the improvement of their PCEs.

The charge collection capability plays an important role in enhancing the PCEs. By inserting a buffer layer between the active layer and electrodes, the energy offset can be overcome and the charge collection capability of the cathode can be enhanced.[16] Selecting an appropriate material for the buffer layer can efficiently reduce the recombination of charges and lower the contact resistance at the electrode interface, which lead to the improvement of charge extraction capability. Consequently, the short circuit current (J_{sc}), open circuit voltage (V_{oc}), and fill factor (FF) can be selectively or even simultaneously enhanced in a single junction device.[17] ZnO has been commonly used as the electron transport layer in inverted PSCs. Thus, by decreasing the energy offset at the ZnO interface, the electron collection capability can be enhanced. Tremendous approaches have been proposed to decrease the energy offset between ZnO and photoactive layers, *e.g.*, introduction of conjugated/non-conjugated polymer electrolytes[18–34] or self-assembled monolayer (SAM)[35–37] treatment at the interface. Lithium or ethoxylated polyethyleneimine (PEIE) doping in the ZnO matrix can improve the PCEs by reducing the defects and traps of the ZnO layer.[38,39] Among them, conjugated polymer electrolytes (CPEs) have been widely used as the cathode buffer layer (CBL). Basically, CPEs consist of a hydrophobic conjugated main chain and hydrophilic polar ionic groups as the side chain. The polar ionic group is directed toward the surface of the ZnO layer and the hydrophobic main chain is directed toward the photoactive layer. Thus, the device performance can be improved by forming an interface dipole through the spontaneous reorganization of polar ionic groups.[40–44]

Poly[(9,9-bis(3′-(*N*,*N*-dimethylamino)propyl)-2,7-fluorene)-*alt*-2,7-(9,9-dioctylfluorene)] (PFN) has been widely used in electroluminescent devices[45,46] as an emitter and CBL for PSCs when compared with other CPEs.[47–52] This polymer can be dissolved in common solvents such as chlorinated hydrocarbon,

[a]*Department of Polymer Engineering, Pukyong National University, Busan 48513, Korea. E-mail: jkim@pknu.ac.kr*

[b]*Division of Chemical Engineering, Konkuk University, Seoul 05029, Korea*

† Electronic supplementary information (ESI) available. See DOI: 10.1039/c9ta12931f

‡ H. C. Jin and S. A. Salma equally contributed to this research.

tetrahydrofuran (THF), toluene, or xylene. Therefore, it is difficult to construct multi-layer structured devices because of the poor solvent resistance of the successive layer coating. However, quaternarizing PFN with alkyl bromide (bromoethane or bromomethane) or adding a small amount of acetic acid (AA) to PFN can alter its intrinsic solubility. Both quaternarized PFN and PFN modified with AA were readily soluble in polar solvents such as methanol, ethanol, *N*,*N*-dimethylformamide, and dimethylsulfoxide. These treatments allow the application of PFN to fabricate multi-layer structured devices. A typical degree of quaternarization for PFN is less than 90%[45,51] even after a long quaternarization reaction time (a week or longer). PFN salts are easily formed by a simple acid–base reaction of AA with the tertiary amine group in the side chain of PFN. These salts do not dissolve in chlorinated hydrocarbon, THF, toluene, or xylene. Therefore, adding AA into the PFN matrix is convenient for preparing insoluble films with solvent resistance on the successive layer coating. However, it is necessary to systematically study the effect of the amount of added AA on the device performance because an excess of AA in the PFN layer can destroy the device. Polyelectrolytes with different counter anions have also been used to enhance the electron injection/collection ability at the cathode interface.[22,53,54] Therefore, it is necessary to study the effect of the type of acid additive on the photovoltaic properties to understand the role of the counter anion of acid derivatives. In this study, we report the photovoltaic properties of inverted PSCs (shown in Fig. 1b and c) based on PFN with different amounts and types of acid derivatives (shown in Fig. 1a) as the CBL. To the best of our knowledge, the effect of the amount and type of acid additive in the PFN interlayer on photovoltaic properties has never been reported before.

Results and discussion

We used X-ray photoelectron spectroscopy (XPS) to analyze the presence of acid derivatives on the ZnO surface. Fig. 2a shows the survey spectra of acid derivatives on the ZnO surface. The peaks at 530, 400, and 285 eV in the survey spectra correspond to O 1s, N 1s, and C 1s, respectively. The peak at 688 eV in the XPS spectra of ZnO/PFN-CF3BA and ZnO/PFN-CF3AA corresponds to F 1s (Fig. 2b). As shown in Fig. 2c, the peak at 169 eV in the XPS spectrum of ZnO/PFN-TsOH corresponds to S 2p. The presence of the acid–base reaction product of PFN and acid derivatives was confirmed by the XPS spectra. The peaks at 1045 and 1021 eV (Fig. S1a†) correspond to Zn $2p_{1/2}$ and Zn $2p_{3/2}$, respectively. The position of the corresponding peaks in ZnO

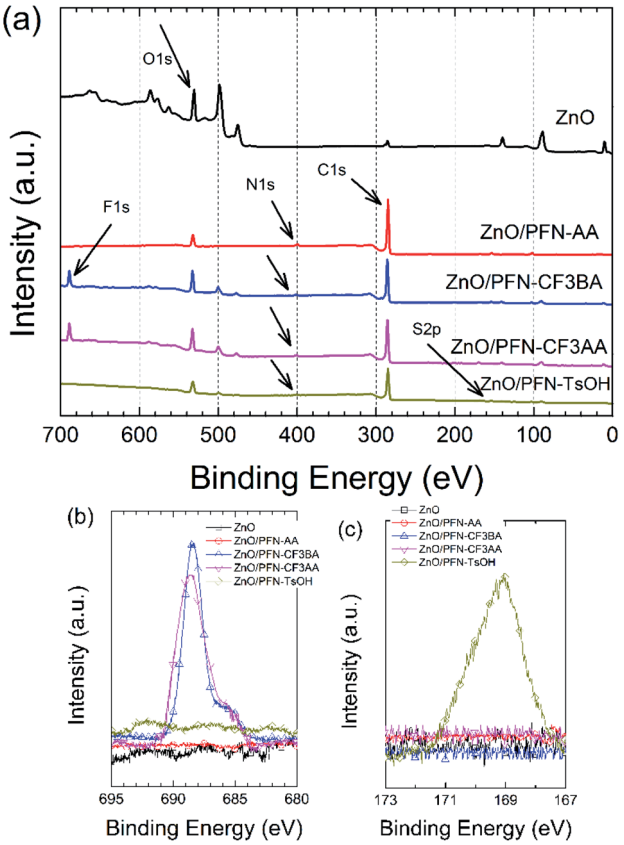

Fig. 2 (a) XPS survey spectra, and (b) F 1s and (c) S 2p spectra of ZnO and ZnO/PFN with 1.0 eq. of acid derivatives.

with diverse acid-modified PFNs was shifted to higher binding energy than those in the spectrum of pristine ZnO. This means that the change in the surroundings of the Zn atoms has become more electron rich compared to pristine ZnO. The peaks at 532 and 530 eV (Fig. S1b†) in the XPS spectrum of ZnO were assigned to oxygen in the OH group and in ZnO, respectively. The number of defect sites in ZnO cannot be estimated from the intensity of the OH peak because the peak at 532 eV originated from the ZnO and acid derivatives simultaneously.

The equilibrium constant (K) of the reaction between PFN and different types of acid derivatives (shown in Fig. 3) can be estimated by using $K = 10^{(pK_a(PFN\text{-}H^+A^-) - pK_a(A\text{-}H))}$, where pK_a(A–H) is the pK_a value of the acid derivative and pK_a(PFN-H$^+$A$^-$) is the pK_a value of PFN-H$^+$. Assuming that PFN-H$^+$ is equivalent to

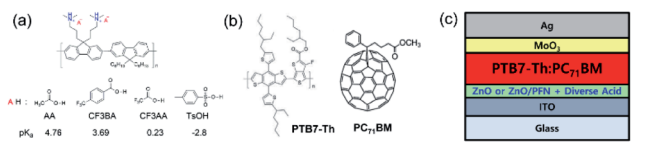

Fig. 1 Chemical structure of (a) PFN with diverse acid derivatives, (b) PTB7-Th and $PC_{71}BM$, and (c) the device structure of the OSC used in this study.

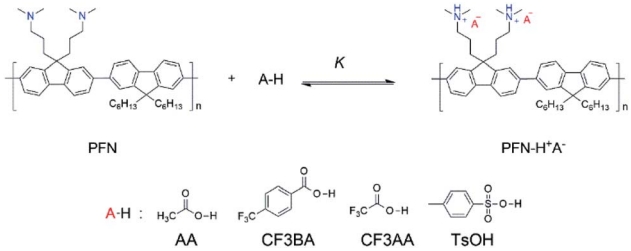

Fig. 3 Reaction between PFN and acid derivatives.

a trialkyl ammonium salt and its pK_a value is 10.75, the K values of acid–base reactions between PFN and different types of acid derivatives were estimated to be 1.0×10^6, 1.2×10^7, 3.3×10^{10}, and 3.6×10^{13} for AA, CF3BA, CF3AA, and TsOH, respectively. Thus, it was confirmed that all the trialkyl amine in the side chains was completely converted to a trialkyl ammonium salt by the addition of acid derivatives such as AA, CF3BA, CF3AA, and TsOH.

Fig. S2† shows the static water contact angle (SWCA) measurement data of the ZnO surface and ZnO surface with PFN-acid derivatives. The SWCA of the ZnO surface with PFN added with 1.0 equivalent (eq.) of acid derivatives is larger than that of the ZnO surface (19.08°) because the ZnO surface with PFN-acid derivatives becomes more hydrophobic when compared with the pristine ZnO surface. Because of the high hydrophobic nature of fluorine atoms, the ZnO surface with PFN-CF3BA and PFN-CF3AA exhibited a larger SWCA when compared with the others. The SWCA data can be well related to the physical properties of PFN-acid derivatives, which might affect the photovoltaic properties of PSCs with different combinations of acid derivatives and PFN as the CBL.

We fabricated inverted type PSCs (ITO/ZnO/PFN with acid derivatives/PTB7-Th:$PC_{71}BM$/MoO_3/Ag) to investigate the effect of different types of acid derivatives on the photovoltaic properties. Several different amounts of acid derivatives ranging from 0.5 to 6.0 eq. were tested to detect the optimum concentration of acid derivatives (see Table 1). We noticed that the devices with PFN added with 1.0 eq. of acid derivative exhibited the highest PCE. As for AA, the amount of AA did not significantly affect the PCE of the devices. Besides, an excess of CF3BA and TsOH did not significantly affect the PCE. This is presumably because these acid derivatives are in the solid state. However, the PCE of the devices with PFN added with 6.0 eq. of acid derivative was excessively lower when compared with the other types of devices. As shown in Fig. S3,† the surface roughness of ZnO/PFN with 6.0 eq. of CF3AA was 5.39 nm, which was excessively larger than that of ZnO/PFN with 1.0 eq. of CF3AA (3.02 nm). This is because the excess of liquid CF3AA may deteriorate the ZnO layer. Fig. 4a and b display the current density–voltage (J–V) curves of the PSCs with PFN added with an optimum amount of acid derivatives that exhibit the highest PCE under illumination and the J–V curves under dark conditions; their photovoltaic parameters are summarized in Table 1. The PCEs of the devices with AA, CF3BA, CF3AA, and TsOH were 9.9% (short circuit current (J_{sc}) = 18.8 mA cm^{-2}, open circuit voltage (V_{oc}) = 0.80 V, and fill factor (FF) = 66.5%), 10.3% (J_{sc} = 18.8 mA cm^{-2}, V_{oc} = 0.81 V, and FF = 68.2%), 10.3% (J_{sc} = 18.4 mA cm^{-2}, V_{oc} = 0.81 V, and FF = 69.5%), and 10.6% (J_{sc} = 18.7 mA cm^{-2}, V_{oc} = 0.80 V, and FF = 70.6%), respectively, whereas the PCE of the device with pristine ZnO was 8.7% with J_{sc} = 17.7 mA cm^{-2}, V_{oc} = 0.80 V, and FF = 61.4%. Thus, it is evident that a significant improvement can be obtained using the device based on ZnO/PFN with 1.0 eq. of acid derivatives. The PCEs of the PSCs based on ZnO/PFN with 1.0 eq. of AA, CF3BA, CF3AA, and TsOH were improved by 15.0, 18.9, 18.2, and 21.4%, respectively, when compared with the PSC based on pristine ZnO.

The relative enhancement of J_{sc} of the PSCs based on ZnO/PFN-AA (1.0 eq.), ZnO/PFN-CF3BA (1.0 eq.), ZnO/PFN-CF3AA (1.0 eq.), and ZnO/PFN-TsOH (1.0 eq.) was 6.28, 6.51, 3.96 and 5.77%, respectively, when compared with the PSC with pristine ZnO. And the relative enhancement of FFs of the PSCs with ZnO/PFN-AA (1.0 eq.), ZnO/PFN-CF3BA (1.0 eq.), ZnO/PFN-CF3AA (1.0 eq.), and ZnO/PFN-TsOH (1.0 eq.) was 8.3, 11.1, 13.2 and 15.0%, respectively, when compared with the PSC with pristine ZnO. The main contributing factor for the enhancement of efficiency was the improvement of J_{sc} and FF, simultaneously. In order to understand the trend of the J_{sc} of the PSCs, we performed Kelvin probe microscopy (KPM) measurements of ZnO and PFN-modified ZnO. KPM is a well-known powerful tool for

Table 1 Photovoltaic parameters of PSCs based on ZnO/PFN with different types and amounts of acid derivatives; PFN-diverse acid exhibits the highest PCE. The averages and deviations (20 devices) are shown in parentheses

ETL	Amount of acid to PFN	J_{sc} (mA cm^{-2})	V_{oc} (V)	FF (%)	PCE (%)	[a]Calculated J_{sc} (mA cm^{-2})
ZnO	—	17.7 (17.53)	0.80 (0.80)	61.4 (60.9)	8.7 (8.5)	17.5
ZnO/PFN-AA	0.5 eq.	18.1 (18.0)	0.81 (0.80)	67.0 (66.9)	9.8 (9.6)	—
	1.0 eq.	18.8 (18.6)	0.80 (0.80)	66.5 (66.1)	9.9 (9.8)	18.0
	1.5 eq.	18.4 (18.3)	0.81 (0.80)	67.2 (66.4)	9.9 (9.8)	—
	6.0 eq.	18.2 (18.2)	0.80 (0.80)	66.8 (66.2)	9.7 (9.6)	—
ZnO/PFN-CF3BA	0.5 eq.	18.7 (18.6)	0.81 (0.81)	68.2 (66.8)	10.3 (10.1)	—
	1.0 eq.	18.8 (18.7)	0.81 (0.80)	68.2 (67.4)	10.3 (10.1)	18.8
	1.5 eq.	18.3 (18.22)	0.80 (0.80)	61.5 (60.7)	9.0 (8.9)	—
	6.0 eq.	17.8 (17.7)	0.78 (0.78)	57.8 (57.6)	8.0 (7.9)	—
ZnO/PFN-CF3AA	0.5 eq.	18.0 (17.8)	0.81 (0.81)	68.8 (68.0)	10.0 (9.8)	—
	1.0 eq.	18.4 (18.3)	0.81 (0.80)	69.5 (69.0)	10.3 (10.2)	18.5
	1.5 eq.	17.9 (17.8)	0.80 (0.79)	67.4 (67.0)	9.7 (9.5)	—
	6.0 eq.	15.0 (11.9)	0.39 (0.35)	21.6 (19.1)	1.3 (0.83)	—
ZnO/PFN-TsOH	0.5 eq.	18.5 (18.4)	0.81 (0.80)	68.3 (67.2)	10.2 (10.1)	—
	1.0 eq.	18.7 (18.6)	0.80 (0.80)	70.6 (69.7)	10.6 (10.4)	18.7
	1.5 eq.	18.2 (18.0)	0.81 (0.81)	67.6 (66.3)	9.9 (9.8)	—
	6.0 eq.	17.3 (17.2)	0.79 (0.79)	58.9 (56.8)	8.1 (7.7)	—

[a] Calculated from the IPCE spectra.

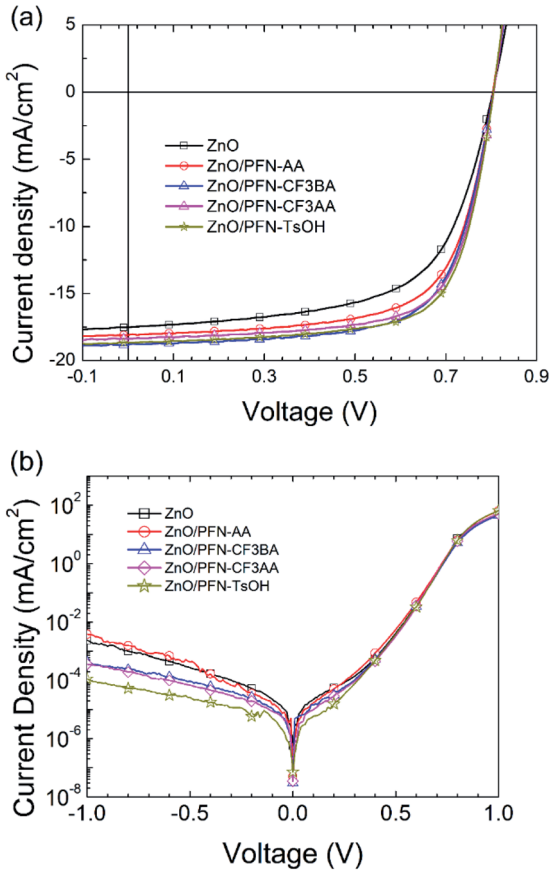

Fig. 4 Current density–voltage curves of PSCs based on ZnO and ZnO/PFN with 1.0 eq. of acid derivatives (a) under illumination and (b) under dark conditions.

investigating the work function of metals or semiconductors. The work function of ZnO/PFN-AA (1.0 eq.), ZnO/PFN-CF3BA (1.0 eq.), ZnO/PFN-CF3AA (1.0 eq.), and ZnO/PFN-TsOH (1.0 eq.) was –4.09, –4.11, –4.07, and –4.06 eV, respectively, which are higher than that of pristine ZnO (−4.29 eV). Thus, the energy offset at the interface was reduced by the thin layer of PFN with diverse acid derivatives. The reduction of the energy barrier at the interface will promote the electron collection capability. Thus, the J_{sc} values of the devices with ZnO with PFN with diverse acid derivatives were better than that of the device with pristine ZnO. The work function data agree well with the trend of J_{sc}. Noticeably, the trend of J_{sc} data and the work function were not significantly dependent on the type of acid derivative. Interestingly, the PCE and FF of the devices follow the trend of the pK_a value of acid derivatives.

The series resistance (R_s) and shunt resistance (R_{sh}) were obtained from the *J–V* curves obtained under dark and 1.0 sun conditions (summarized in Table 2). The R_s of the devices with ZnO/PFN-AA, ZnO/PFN-CF3BA, ZnO/PFN-CF3AA, and ZnO/PFN-TsOH under dark conditions was 2.64, 2.59, 2.48, and 2.12 Ω cm^2, respectively, and they are smaller than that of the device with ZnO (3.02 Ω cm^2). The R_s values of the devices under 1.0 sun conditions were higher than those under dark conditions and follow the trend of the R_s data under dark conditions. The obtained R_s data support the trends of FF and PCE. The J_{sc} data calculated from the incident photon-to-current efficiency (IPCE) curves (see Fig. S4†) of the devices agreed well with the J_{sc} of the devices. The shunt resistance (R_{sh}) of the devices with ZnO/PFN-AA, ZnO/PFN-CF3BA, ZnO/PFN-CF3AA, and ZnO/PFN-TsOH under 1.0 sun conditions was 0.83, 1.00, 1.02, and 1.10 kΩ cm^2, respectively, which are higher than that of the device with pristine ZnO (0.58 kΩ cm^2). The R_{sh} data under illumination are well coherent with the FF of the devices.

To determine the carrier recombination and transport mechanism, we acquired the electrical impedance spectra (EIS) of the PSCs with ZnO and ZnO/PFN with 1.0 eq. of AA, CF3BA, CF3AA, and TsOH, respectively under dark conditions. The EIS measurements were performed under dark conditions at different applied voltages with a frequency ranging from 1 Hz to 1.0 MHz. Fig. 5a shows the Nyquist plots of the devices at 0 V. In our results, a single semi-circle without the transmission line was observed in the Nyquist plots of each device. The transmission line is generally observed when the transport resistance is smaller than the recombination resistance (R_{rec}), indicating efficient charge collection. In the case of strong recombination, the EIS spectra followed the Gerischer impedance model. The absence of a transmission line indicates that the devices experience strong recombination.[55–61] In addition, the diameter of the semi-circle has been assigned as charge transfer resistance.[62–71]

The size of the EIS semi-circle reflects the extent of R_{rec}. Thus, the arc size in EIS depends on the extent of charge recombination in PSCs. The magnitude of R_{rec} of the devices was in the order: ZnO (1150 kΩ) < ZnO/PFN-AA (1490 kΩ) < ZnO/PFN-CF3BA (1890 kΩ) < ZnO/PFN-CF3AA (2350 kΩ) < ZnO/PFN-TsOH (2365 kΩ). By introducing acid-modified PFN as the CBL, the size of the semi-circle is increased, leading to increased R_{rec},

Table 2 The series and shunt resistance of the device under dark and 1.0 sun conditions

ETL	Amount of acid to PFN	R_s[a] (Ω cm^2)	R_s[b] (Ω cm^2)	R_{sh}[c] (kΩ cm^2)
ZnO	—	3.02	6.27	0.58
ZnO/PFN-AA	1.0 eq.	2.64	5.15	0.83
ZnO/PFN-CF3BA	1.0 eq.	2.59	4.69	1.00
ZnO/PFN-CF3AA	1.0 eq.	2.48	4.28	1.02
ZnO/PFN-TsOH	1.0 eq.	2.12	4.11	1.10

[a] Series resistance under dark conditions. [b] Series resistance under 1.0 sun conditions. [c] Shunt resistance under 1.0 sun conditions.

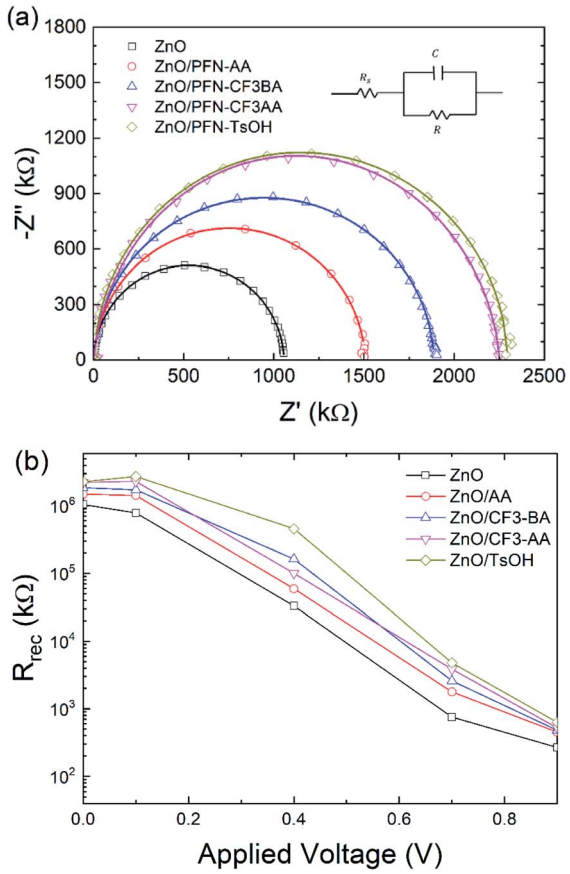

Fig. 5 (a) EIS spectra; the inset shows the equivalent circuit for the analysis of EIS spectra (R_s: ohmic resistance including the electrode and bulk resistance, R: resistance associated with the interface charge transport, and C: capacitance), and (b) calculated recombination resistance *vs.* applied voltage.

and thus the recombination at the interface is suppressed. Noticeably, the device based on TsOH modified PFN exhibited the highest R_{rec} among the acid derivatives, indicating the lowest reduced interfacial recombination. This can be well related to the FFs of the PSCs.

Fig. 5b shows R_{rec} as a function of applied voltage under dark conditions. It should be noticed that with an increase in the applied voltage, the R_{rec} gradually decreased. This is due to the fact that the extraction of charge is hindered at a high applied voltage. The R_{rec} of the devices based on acid-modified PFN at each applied voltage exhibited higher values than that of the device with pristine ZnO. This result confirms that the devices with acid-modified PFN lower the charge recombination during charge transfer and transport.[72] Among the devices, the device with TsOH modified PFN exhibited the highest R_{rec} at various applied voltages. Fig. S5† shows the Nyquist plots of the devices at 0 V under 1.0 sun conditions. The R_{rec} of the devices based on ZnO, ZnO/PFN-AA, ZnO/PFN-CF3BA, ZnO/PFN-CF3AA, ZnO/PFN-TsOH was 3.69, 6.35, 6.69, 7.14, and 7.21 kΩ, respectively. They are well coherent with the R_{sh} data under illumination and follow the trend of R_{rec} under dark conditions. The magnitude of R_{rec} of the devices under 1.0 sun conditions was significantly smaller than those of the devices under dark conditions. This is due to the fact that the photo-induced charge carriers lower the R_{rec} of the devices.

To elaborate the electron transport properties of the ZnO layer, electron only devices (ITO/ZnO/PFN with 1.0 eq. of AA, CF3BA, CF3AA, or TsOH/$PC_{71}BM$ (60 nm)/Al (100 nm)) (Fig. S6†) were fabricated and tested. The electron mobility of the device was calculated by using the Mott–Gurney equation.[54] The electron mobility of the devices based on ZnO/PFN with 1.0 eq. of AA, CF3BA, CF3AA, and TsOH was 2.73×10^{-3}, 3.30×10^{-3}, 3.33×10^{-3}, and 3.34×10^{-3} $cm^2\ V^{-1}\ s^{-1}$, respectively. They are higher than that of the device based on pristine ZnO (2.24×10^{-3} $cm^2\ V^{-1}\ s^{-1}$).[73] Thus, the J_{sc} data of the devices based on ZnO with acid-modified PFN were improved compared to that of the device with pristine ZnO. But, the change in mobility data is not significantly dependent on the type of acid derivative. This is one possible reason for the J_{sc} data not being significantly dependent on the type of acid derivative.

Furthermore, we evaluated the relationship between the photocurrent density (J_{ph}) and effective voltage (V_{eff}) to realize the charge transport and collection properties of the devices. The J_{ph} and V_{eff} can be defined as J_L (current density under illumination) $- J_D$ (current density under dark conditions) and V_0 (voltage at $J_{ph} = 0$) $- V_a$ (applied voltage), respectively. As shown in Fig. S7,† the V_{eff} values in the saturated photocurrent regime (V_{sat}) of the device based on pristine ZnO and ZnO/PFN with 1.0 eq. of AA, CF3BA, CF3AA, and TsOH were 0.20, 0.18, 0.18, 0.16, and 0.15 V. Noticeably, the trend of saturated voltage agrees with the change of J_{sc} of the PSCs because a smaller V_{sat} indicates a faster transition from the space-charge-limited regime to the saturation regime.

The saturation current density (J_{sat}) can be correlated with the maximum exciton generation rate (G_{max}), exciton dissociation probability, and carrier transport and collection probability at high V_{eff}. The G_{max} was calculated by using the equation J_{ph}/qL, where q and L are the electron charge and thickness of the active layer, respectively. G_{max} is related to the absorption of light by the active layer.[74] The G_{max} under the J_{sat} conditions of the devices based on pristine ZnO and ZnO/PFN with 1.0 eq. of AA, CF3BA, CF3AA, and TsOH was 1.60×10^{28}, 1.61×10^{28}, 1.68×10^{28}, 1.64×10^{28}, and 1.66×10^{28} $cm^{-3}\ s^{-1}$, respectively. No significant changes in G_{max} were observed because the G_{max} is dependent on the absorbance of the active layer. The J_{sat} is limited by the carrier transport and collection, when all the photo-generated excitons are dissociated into free charge carriers at high V_{eff}. Thus, the carrier transport and collection probability at any V_{eff} can be estimated from the ratio of J_{ph}/J_{sat}. The saturation current density (J_{sat}) is estimated from the convergent value of J_{ph}. The J_{ph}/J_{sat} values of the PSCs with ZnO/PFN with 1.0 eq. of AA, CF3BA, CF3AA, and TsOH were 94.1, 94.5, 94.9, and 95.2%, respectively, which are higher than that of the device based on pristine ZnO (90.1%). This is due to the fact that the acid-modified PFN improves the carrier transport and collection of the devices. The trend of J_{ph}/J_{sat} data of the devices with acid-modified ZnO follows the trend of the performances of the devices.

To realize the charge recombination kinetics at the interfaces further, we investigated the J_{sc} and V_{oc} of the devices as a function of illumination intensity.[75–77] The relationship between J_{sc} and illumination intensity is generally defined as $J_{sc} \propto I^{\alpha}$, where I is the illumination intensity. When α is 1, the devices exhibit completely bimolecular recombination under short-circuit conditions. As shown in Fig. 6a, the α of the devices based on ZnO/PFN with 1.0 eq. of AA, CF3BA, CF3AA, and TsOH was 0.98, 0.98, 0.98, and 0.97, respectively, which are comparable to that of the device based on ZnO (0.96). This indicates that the devices exhibited slight bimolecular recombination because of the decreased space charge at the interfaces. However, the α values were not dependent on the type of acid derivative. These results match well with the trend of J_{sc} and electron mobility of the devices.

Fig. 6b displays V_{oc} as a function of illumination intensity (I). The relationship between V_{oc} and illumination intensity is defined as $V_{oc} \propto skT/q \ln(I)$, where k, T, and q are the Boltzmann constant, temperature in Kelvin, and electron charge, respectively. If the device has only the trap-assisted recombination channel, then the s value will be 2. If the device has only the band-to-band recombination, then the s value will be 1. The s values of the devices based on ZnO/PFN with 1.0 eq. of AA, CF3BA, CF3AA, and TsOH were estimated to be 1.36, 1.28, 1.16, and 1.12, respectively, which are smaller than that of the device with pristine ZnO (1.37). Thus, the devices exhibited reduced trap-assisted recombination. Note that the change in the s values of the devices agrees well with the trend of the PCEs of PSCs and follows the trend of the pK_a value of acid derivatives.

Furthermore, the devices were kept in a nitrogen-filled glove box without passivation. After 800 hours, the PCEs of the devices based on ZnO and ZnO/PFN with 1.0 eq. of AA, CF3BA, CF3AA, and TsOH were found to be 97, 97, 94, 97, and 96% of their initial PCEs. The acidity of the additives did not significantly affect the device stability. However, the devices with excess acid derivatives exhibited poor stability when compared with the devices with 1.0 eq. of acid derivatives. The PCEs of the devices after 800 hours with 1.0 eq. of AA, CF3BA, CF3AA, and TsOH were found to be 88, 89, 90, 87, and 89% of their initial PCEs. The PCE of the device based on ZnO after 800 hours was 91%. This is presumably because the excess of acid derivatives destroys the devices.

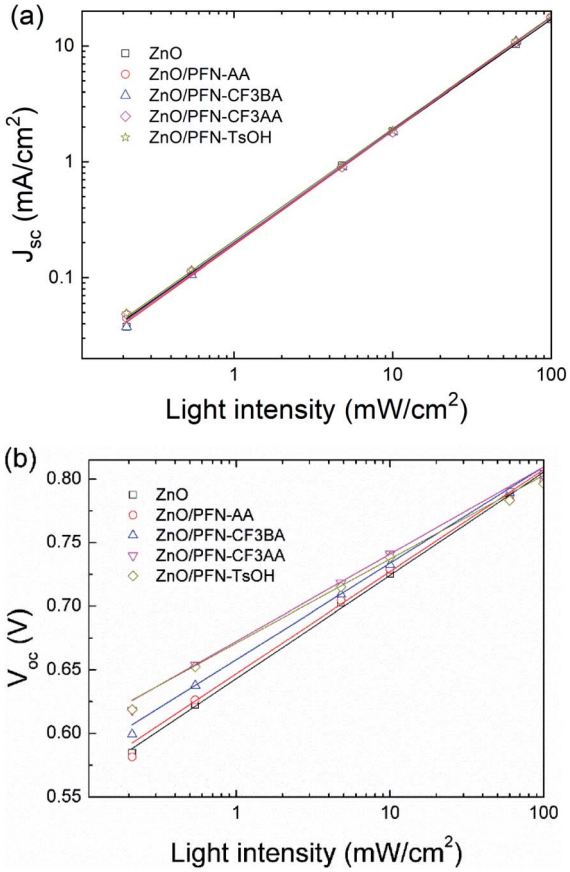

Fig. 6 (a) J_{sc} and (b) V_{oc} *vs.* light intensity plots of the PSCs.

Experimental

Materials

All chemicals were purchased from Alfa Aesar or Sigma-Aldrich and used as received unless otherwise described. Poly([2,6′-4,8-di(5-ethylhexylthienyl)benzo[1,2-*b*;3,3-*b*]dithiophene]{3-fluoro-2[(2-ethylhexyl)carbonyl]thieno[3,4-*b*]thiophenediyl}) (PTB7-Th) and $PC_{71}BM$ ([6,6]-phenyl C71 butyric acid methyl ester) were purchased from Derthon Optoelectronic Materials Science Technology Co. Ltd. Poly[(9,9-bis(3′-(*N*,*N*-dimethylamino) propyl)-2,7-fluorene)-*alt*-2,7-(9,9-dihexylfluorene)] (PFN) was synthesized by the literature procedures.[43,44] And the rest of the experimental details for the static water contact angle, AFM, IPCE, EIS, and *J*–*V* curves of electron only devices, and J_{ph} *vs.* V_{eff} curves of the devices are available in the ESI.†

Conclusions

To systematically study the effect of acid additives such as AA, CF3BA, CF3AA, and TsOH in PFN on device performance, we fabricated and tested inverted PSCs that use a blend of PTB7-Th and $PC_{71}BM$ as the active layer and PFN with different amounts and types of acid derivatives as the CBL. The optimum amount of acid derivatives was found to be 1.0 eq. for all the devices based on ZnO/PFN. The PCEs of the devices with 1.0 eq. of AA, CF3BA, CF3AA, and TsOH were 9.9, 10.3, 10.3, and 10.6%, respectively, whereas the PCE of the device with pristine ZnO was 8.7%. The main contributing factor for the enhancement of PCE was the improvement of J_{sc} and FF, simultaneously. The trend of J_{sc} data and the work function were not significantly dependent on the type of acid derivative. The FF and PCEs of the devices followed the trend of the acid dissociation constant of acid derivatives. We discovered that the most effective acid derivative was TsOH in this study. The devices based on PFN with acid derivatives exhibited reduced trap-assisted recombination and interfacial bimolecular recombination. Notably, the reduced trap-assisted recombination of the devices agrees well with the trend of the PCEs of PSCs and follows the trend of the acid dissociation constant of acid derivatives.

Conflicts of interest

There are no conflicts to declare.

Acknowledgements

This research work was supported by the New & Renewable Energy Core Technology Program of the Korea Institute of Energy Technology Evaluation and Planning (KETEP) granted financial resource from the Ministry of Trade, Industry & Energy, Republic of Korea (20182010106360A and 20193091010110).

Notes and references

1 X. Li, X. Liu, W. Zhang, H.-Q. Wang and J. Fang, *Chem. Mater.*, 2017, **29**, 4176–4180.
2 Z. Wu, C. Sun, S. Dong, X.-F. Jiang, S. Wu, H. Wu, H.-L. Yip, F. Huang and Y. Cao, *J. Am. Chem. Soc.*, 2016, **138**, 2004–2013.
3 M. Lv, S. Li, J. J. Jasieniak, J. Hou, J. Zhu, Z. Tans, S. E. Watkins, Y. Li and X. Chen, *Adv. Mater.*, 2013, **25**, 6889–6894.
4 C. J. Brabec, A. Cravino, D. Meissner, N. S. Sariciftci, T. Fromherz, M. T. Rispens, L. Sanchez and J. C. Hummelen, *Adv. Funct. Mater.*, 2001, **11**, 374–380.
5 Y. Li, *Acc. Chem. Res.*, 2012, **45**, 723–733.
6 W. Zhang, Y. Wu, Q. Bao, F. Gao and J. Fang, *Adv. Energy Mater.*, 2014, **4**, 1400359.
7 G. Yu, J. Gao, J. C. Hummelen, F. Wudl and A. J. Heeger, *Science*, 1995, **270**, 1789–1791.
8 M. H. Hoang, G. E. Park, D. L. Phan, T. T. Ngo, T. V. Nguyen, C. G. Park, M. J. Cho and D. H. Choi, *Macromol. Res.*, 2018, **26**, 844–850.
9 Y. J. Lee, S. J. Jeon, J. Y. Choi and D. K. Moon, *J. Ind. Eng. Chem.*, 2019, **75**, 138–147.
10 B. Zhu, X. Chen, S. I. Huang and X. Peng, *Dyes Pigm.*, 2019, **164**, 148–155.
11 S. S. Badge, H. Park, V. H. Tran and S. H. Lee, *Dyes Pigm.*, 2019, **163**, 30–39.
12 S. J. Jeon, J. E. Yu, Y. W. Han, I. S. Suh and D. K. Moon, *J. Ind. Eng. Chem.*, 2019, **71**, 137–147.
13 E. R. Rwenyagila, *Int. J. Photoenergy*, 2017, **2017**, 1–12.
14 L. J. A. Koster, E. C. P. Smits, V. D. Mihailetchi and P. W. M. Blom, *Phys. Rev. B: Condens. Matter Mater. Phys.*, 2005, **72**, 085205.
15 Y.-J. Cheng, S.-H. Yang and C.-S. Hsu, *Chem. Rev.*, 2009, **109**, 5868–5923.
16 H.-L. Yip and A. K.-Y. Jen, *Energy Environ. Sci.*, 2012, **5**, 5994–6011.
17 T. T. Do, H. S. Hong, Y. E. Ha, S. I. Yoo, Y. S. Won, M.-J. Moon and J. H. Kim, *Macromol. Res.*, 2015, **23**, 367–376.
18 S.-H. Oh, S.-I. Na, J. Jo, B. Lim, D. Vak and D.-Y. Kim, *Adv. Funct. Mater.*, 2010, **20**, 1977–1983.
19 S. Nho, G. Baek, S. Park, B. R. Lee, M. J. Cha, D. C. Lim, J. H. Seo, S.-H. Oh, M. H. Song and S. Cho, *Energy Environ. Sci.*, 2016, **9**, 240–246.
20 Y. Sun, J. H. Seo, C. J. Takacs, J. Seifter and A. J. Heeger, *Adv. Mater.*, 2011, **23**, 1679–1683.
21 C. E. Small, S. Chen, J. Subbiah, C. M. Amb, S.-W. Tsang, T.-H. Lai, J. R. Reynolds and F. So, *Nat. Photon.*, 2012, **6**, 115–120.
22 M. Y. Jo, Y. E. Ha and J. H. Kim, *Sol. Energy Mater. Sol. Cells*, 2012, **107**, 1–8.
23 M. Y. Jo, Y. E. Ha and J. H. Kim, *Org. Electron.*, 2013, **14**, 995–1001.
24 G. E. Lim, Y. E. Ha, M. Y. Jo, J. Park, Y.-C. Kang and J. H. Kim, *ACS Appl. Mater. Interfaces*, 2013, **5**, 6508–6513.
25 Y. Li, X. Liu, X. Li, W. Zhang, F. Xing and J. Fang, *ACS Appl. Mater. Interfaces*, 2017, **9**, 8426–8431.
26 Z. Li, Q. Chen, Y. Liu, L. Ding, K. Zhang, K. Zhu, L. Yuan, B. Dong, Y. Zhou and B. Song, *Macromol. Rapid Commun.*, 2018, **39**, 1700828.
27 Y. H. Kim, N. Sylvianti, M. A. Marsya, J. Park, Y.-C. Kang, D. K. Moon and J. H. Kim, *ACS Appl. Mater. Interfaces*, 2016, **8**, 32992–32997.
28 Y. H. Kim, N. Sylvianti, M. A. Marsya, D. K. Moon and J. H. Kim, *Org. Electron.*, 2016, **39**, 163–167.
29 X. Guo, Y. Zhang, X. Liu, S. Braun, Z. Wang, B. Li, Y. Li, C. Duan, M. Fahlman, J. Tang, J. Fang and Q. Bao, *Org. Electron.*, 2018, **59**, 15–20.
30 J. P. Han, E. J. Lee, Y. W. Han, T. H. Lee and D. K. Moon, *J. Ind. Eng. Chem.*, 2016, **36**, 44–48.
31 M. Gupta, D. Yan, J. Xu, J. Yao and C. Zhan, *ACS Appl. Mater. Interfaces*, 2018, **10**, 5569–5576.
32 S.-Y. Chang, Y.-C. Lin, P. Sun, Y.-T. Hsieh, L. Meng, S.-H. Bae, Y.-W. Su, W. Huang, C. Zhu, G. Li, K.-H. Wei and Y. Yang, *Sol. RRL*, 2017, **1**, 1700139.
33 S. Shao, K. Zheng, T. Pullerits and F. Zhang, *ACS Appl. Mater. Interfaces*, 2013, **5**, 380–385.
34 S. Park, W. Jang, J. A. Cho and M. Yi, *J. Ind. Eng. Chem.*, 2018, **61**, 314–320.
35 H.-C. Chen, S.-W. Lin, J.-M. Jiang, Y.-W. Su and K.-H. Wei, *ACS Appl. Mater. Interfaces*, 2015, **7**, 6273–6628.
36 S.-H. Liao, H.-J. Jhuo, Y.-S. Cheng and S.-A. Chen, *Adv. Mater.*, 2013, **25**, 4766–4771.
37 H. Yang, T. Wu, T. Hu, X. Hu, L. Chen and Y. Chen, *J. Mater. Chem. C*, 2016, **4**, 8738–8744.
38 A. Soultati, A. Fakharuddin, E. Polydorou, C. Drivas, A. Kaltzoglou, M. I. Haider, F. Kournoutas, M. Fakis, L. C. Palilis, S. Kennou, D. Davazoglou, P. Falaras, P. Argitis, S. Gardelis, A. Kordatos, A. Chroneos, L. Schmidt-Mende and M. Vasilopoulou, *ACS Appl. Energy Mater.*, 2019, **2**, 1663–1675.
39 H. Yu, X. Huang and C. Huang, *Appl. Surf. Sci.*, 2019, **470**, 318–330.
40 S.-I. Na, S.-H. Oh, S.-S. Kim and D.-Y. Kim, *Org. Electron.*, 2009, **10**, 496–500.
41 J. Park, R. Yang, C. V. Hoven, A. Garcia, D. A. Fischer, T.-Q. Nguyen, G. C. Bazan and D. M. DeLongchamp, *Adv. Mater.*, 2008, **20**, 2491–2496.
42 Y. Jung, T.-Y. Cho, D. Y. Yoon, C. W. Frank and J. Luning, *Macromolecules*, 2005, **38**, 867–872.

43 M. Y. Jo, Y. E. Ha, Y. S. Won, S. I. Yoo and J. H. Kim, *Org. Electron.*, 2015, **25**, 85–91.
44 M. Y. Jo, T. T. Do, Y. E. Ha, Y. S. Won and J. H. Kim, *Org. Electron.*, 2015, **16**, 18–25.
45 F. Huang, H. Wu, D. Wang, W. Yang and Y. Cao, *Chem. Mater.*, 2004, **16**, 708–716.
46 H. Wu, F. Huang, Y. Mo, W. Yang, D. Wang, J. Peng and Y. Cao, *Adv. Mater.*, 2004, **16**, 1826–1830.
47 Q. Sun, F. Zhang, J. Wang, Q. An, C. Zhao, L. Li, F. Teng and B. Hu, *J. Mater. Chem. A*, 2015, **3**, 18432–18441.
48 E. J. Lee, S. W. Heo, Y. W. Han and D. K. Moon, *J. Mater. Chem. C*, 2016, **4**, 2463–2469.
49 L. Zhang, C. He, J. Chen, P. Yuan, L. Huang, C. Zhang, W. Cai, Z. Liu and Y. Cao, *Macromolecules*, 2010, **43**, 9771–9778.
50 T. Yang, M. Wang, C. Duan, X. Hu, L. Huang, J. Peng, F. Huang and X. Gong, *Energy Environ. Sci.*, 2012, **5**, 8208–8214.
51 B. Liu, W.-L. Yu, Y.-H. Lai and W. Huang, *Macromolecules*, 2002, **35**, 4975–4982.
52 R. Yang, H. Wu, Y. Cao and G. C. Bazan, *J. Am. Chem. Soc.*, 2006, **128**, 14422–14423.
53 T. T. Do, H. S. Hong, Y. E. Ha, J. Park, Y.-C. Kang and J. H. Kim, *ACS Appl. Mater. Interfaces*, 2015, **7**, 3335–3341.
54 A. Bagui and S. S. K. Iyer, *Org. Electron.*, 2014, **15**, 1387–1395.
55 S. Nho, G. Baek, S. Park, B. R. Lee, M. J. Cha, D. C. Lim, J. H. Seo, S.-H. Oh, M. H. Song and S. Cho, *Energy Environ. Sci.*, 2016, **9**, 240–246.
56 H. Liu, L. Huang, X. Cheng, A. Hu, H. Xu, L. Chen and Y. Chen, *ACS Appl. Mater. Interfaces*, 2017, **9**, 1145–1153.
57 Y. Li, X. Li, X. Liu, L. Zhu, W. Zhang and J. Fang, *J. Phys. Chem.*, 2016, **120**, 26244–26248.
58 J. Bisquert, I. Mora-Sero and F. Fabregat-Santiago, *ChemElectroChem*, 2014, **1**, 289–293.
59 V. Gonzalez-Pedro, E. J. Juarez-Perez, W. S. Arsyad, E. M. Barea, F. Fabregat-Santiago, I. Mora-Sero and J. Bisquert, *Nano Lett.*, 2014, **14**, 888–893.
60 V. González-Pedro, X. Xu, I. Mora-Seró and J. Bisquert, *ACS Nano*, 2010, **4**, 5783–5790.
61 R. Kern, R. Sastrawan, J. Ferber, R. Stangl and J. Luther, *Electrochim. Acta*, 2002, **47**, 4213–4225.
62 H. Kim, H. Jeong, T. K. An, C. E. Park and K. Yong, *ACS Appl. Mater. Interfaces*, 2013, **5**, 268–275.
63 H. Wang, G. Liu, X. Li, P. Xiang, Z. Ku, Y. Rong, M. Xu, L. Liu, M. Hu, Y. Yang and H. Han, *Energy Environ. Sci.*, 2011, **4**, 2025–2029.
64 G. Hodes, *J. Phys. Chem. C*, 2008, **112**, 17778–17787.
65 N. Wang, H. Lin, J. Li and X. Li, *Appl. Phys. Lett.*, 2006, **69**, 194104.
66 G.-Q. Han, Y.-R. Liu, W.-H. Hu, B. Dong, X. Li, X. Shang, Y.-M. Chai, Y. –Q. Liu and C. –G. Liu, *J. Electroanal. Chem.*, 2016, **163**, H67–H73.
67 P. Jin, X. Zhang, M. Zhen and J. Wang, *RSC Adv.*, 2016, **6**, 10938–10942.
68 Y. Huang, Y. Li, Z. Hu, G. Wei, J. Guo and J. Liu, *J. Mater. Chem. A*, 2013, **1**, 9809–9813.
69 K. Krishnamoorthy, G. K. Veerasubramani, P. Pazhamalai and S. J. Kim, *Electrochim. Acta*, 2016, **190**, 305–312.
70 Q. Qu, P. Zhang, B. Wang, Y. Chen, S. Tian, Y. Wu and R. J. Holze, *J. Phys. Chem. C*, 2009, **113**, 14020–14027.
71 K. V. Sankar and R. K. Selvan, *RSC Adv.*, 2014, **4**, 17555–17566.
72 L. Contreras, S. Ramos, A. Riquelme, P. Boix, J. Idígoras, I. Mora-Seró and J. A. Anta, *J. Mater. Chem. A*, 2019, **7**, 12191–12200.
73 M. Jeong, H. C. Jin, J. H. Lee and D. K. Moon, *Dyes Pigm.*, 2020, **173**, 107927.
74 X. Jia, Z. Jiang, X. Chen, J. Zhou, L. Pan, F. Zhu, Z. Sun and S. Huang, *ACS Appl. Mater. Interfaces*, 2016, **8**, 3792–3799.
75 F. Yang, Y. Xu, M. Gu, S. Zhou, Y. Wang, K. Lu, Z. Liu, X. Ling, Z. Zhu, J. Chen, Z. Wu, Y. Zhang, Y. Xue, F. Li, J. Yuan and W. Ma, *J. Mater. Chem. A*, 2018, **6**, 17688–17697.
76 R. Azmi, S.-H. Oh and S.-Y. Jang, *ACS Energy Lett.*, 2016, **1**, 100–106.
77 L. J. A. Koster, V. D. Mihailetchi, R. Ramaker and P. W. M. Blom, *Appl. Phys. Lett.*, 2005, **86**, 123509.